On the applicability of carbon nanotubes as nanomechanical probes and manipulators

2012 Nanotechnology 23 415502

(http://iopscience.iop.org/0957-4484/23/41/415502)

Nanotechnology **23** (2012) 415502 (7pp) doi:10.1088/0957-4484/23/41/415502

On the applicability of carbon nanotubes as nanomechanical probes and manipulators

Kai Jin[1,2], Xiqiao Feng[1,2], Tuck Wah Ng[3] and Zhiping Xu[1,2]

[1] Department of Engineering Mechanics, AML, Tsinghua University, Beijing 100084, People's Republic of China
[2] Center for Nano and Micro Mechanics, Tsinghua University, Beijing 100084, People's Republic of China
[3] Laboratory for Optics, Acoustics and Mechanics, Monash University, Clayton, Victoria 3800, Australia

E-mail: xuzp@tsinghua.edu.cn and engngtw@gmail.com

Received 17 July 2012, in final form 26 August 2012
Published 27 September 2012
Online at stacks.iop.org/Nano/23/415502

Abstract
Carbon nanotube (CNT) probes offer improved imaging resolution in atomic force microscopy (AFM) and nanomanipulating devices due to their excellent mechanical properties and high aspect ratios. The basis of ascertaining scanning image quality using CNT probes is often centered on whether axial buckling has occurred or not. Here we explore the mechanical behavior and applicability of CNTs in surface scanning using molecular dynamics simulations in which the influence of van der Waals interactions is accounted for. Our results indicate the possible deleterious effects from van der Waals interaction dominated buckling of the probe, which is exacerbated by surface corrugations at the atomic scale. Under the premise that these issues can be surmounted, a cantilever model developed under known requirements for the structural characteristics of CNT probes is shown to be able to assess imaging fidelity. This model offers an effective guide to the selection and design of CNT probes for AFM.

(Some figures may appear in colour only in the online journal)

1. Introduction

The uniqueness and advantages of the atomic force microscope (AFM) in imaging micro- and nanostructures have been clearly shown over other methods such as optical microscopy (OM), scanning electronic microscopy (SEM), and scanning tunneling microscopy (STM) from the outset [1]. Being able to provide atomic-scale resolution imaging under ambient conditions, the AFM has been widely employed in fields ranging from materials development to the biological sciences. With the rapid development of micro- and nanotechnology and science, imaging techniques with even higher resolutions and over wider spectra (mechanical, chemical, thermal, etc) at the nanoscale are expected to be in high demand in the foreseeable future. However, the resolution of AFM imaging is limited by the convolution effect originating from the finite radius of curvature of the probe tip. This problem is especially critical as the tip is comparable in size with the microstructures of many samples, wherein distortions in scanned images are not uncommon [2]. In order to overcome this limitation, algorithms to reconstruct the surface topography from raw data in measurements have been developed [3, 4]. Nevertheless, problems such as precisely defining contours of the surface and determining the shapes of tips are still encountered with this approach. An alternative, more direct, approach is to use probes with smaller tips. The problem with this is the inherent difficulty in fabricating nanoscale tips with conventional silicon and silicon nitride that will keep their desired mechanical properties intact. Carbon nanotubes (CNTs), on the other hand, have extremely high aspect ratios, high Young's moduli (as high as 1 TPa [5]), and excellent resilience to elastic buckling without the presence of material fracture [6]. For this reason, CNTs attached to the tip of AFM probes have

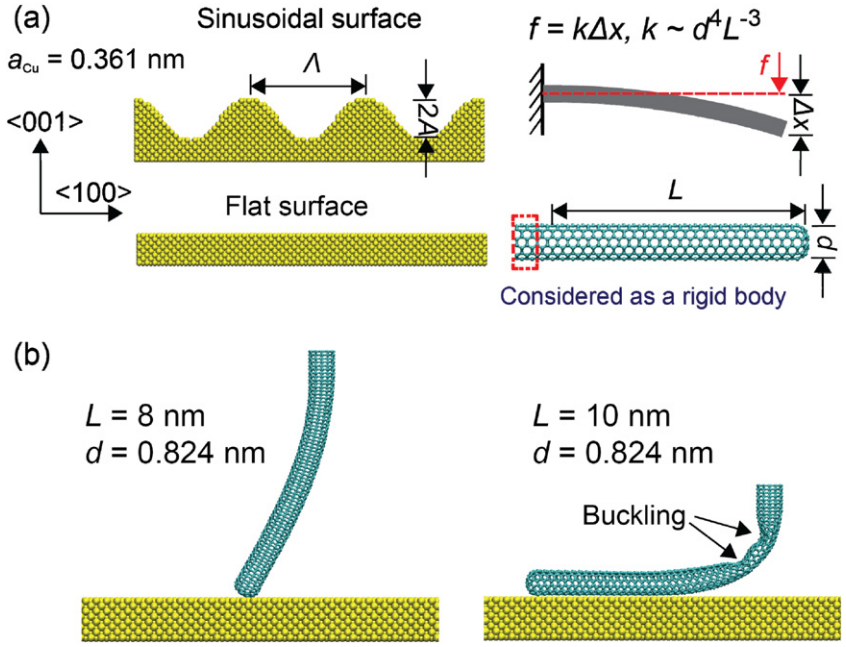

Figure 1. (a) Illustration of the simulation model for the probe–surface system. The target surface is copper (001) with a lattice constant $a_{Cu} = 0.361$ nm. A sinusoidal surface profile defined by its wavelength Λ and amplitude A is introduced to represent an experimental scenario and a flat surface is also introduced to investigate the role of van der Waals interaction. All CNT probes (only one SWNT is shown here for illustration) are capped nanotubes featured by length L and diameter d, among which a top region (highlighted by a dashed box) is considered as a rigid body so as to be loaded in simulations. The probe works like a tip-loaded cantilever in CM scanning, with a stiffness k that relates the force applied and its displacement. (b) Deformation of the CNT during scanning of a flat surface. Bending deformation of the CNT with length $L = 8$ nm is shown, while for $L = 10$ nm, elastic buckling occurs and the CNT lies parallel to the surface.

emerged as a promising technique in AFM imaging [7, 8]. They have been successfully applied in both the tapping mode (TM, where the tip position is recorded as a cantilever oscillator with specific amplitude and frequency) and contact mode (CM, where the tip position is recorded as a cantilever with constant bending displacement) in instruments such as the scanning friction force microscope (SFFM) and scanning nonlinear dielectric microscope (SNDM) [8–13].

The mechanical deformation and stability of CNT probes in an AFM is critical regardless of whether it is operating in the CM or the TM. The validity of measured data is currently often based on the elastic instability of the slender probe condition not being breached, which is a criterion quantified by Euler's elastic buckling theory that gives the critical axial load $F_{cr} = \pi^2 D/4L^2$, where $D = EI$ is the bending rigidity, E the Young's modulus, I the second moment of area, and L the length of the CNT. Yet the van der Waals interaction induced deformation of a CNT can intuitively result in unstable outputs in the TM and imaging distortions in the CM. Compared to that in the TM, the interaction between a CNT tip and the sample surface plays a more important role in the CM. Hence, understanding of the tip behavior during operation is crucial in validating the measured data. Prior to our work, Kutana *et al* [14] explored the response of a single-walled carbon nanotube (SWNT) probe in the TM using molecular dynamics (MD) simulations. Similarities between the prediction and experiment suggest the key role of nonlinear mechanical responses. In contrast to their work, where the reacting force on the SWNT was calculated at specific probe–surface distances, we focus on the deformation response as in the CM, where reacting forces are maintained as a constant. Moreover, factors accounting for the imaging quality are discussed in detail here using results from our MD simulations. In our MD simulations, CNTs with various geometric parameters (diameters, lengths, etc) are investigated and mapped to their performance as scanning tips. From these results, techniques to minimize imaging distortions in measurements can be outlined.

2. Models and methods

The atomic structures of both probes and sample surfaces used in our simulations are illustrated in figure 1(a). A (001) surface of a copper sample is constructed and scanned with a CNT probe. The surface is considered to be rigid and vibrational effects are not included in our simulations. A sinusoidal function is chosen as the profile of a copper surface in the ⟨100⟩ direction, in order to represent surface corrugation of sample surfaces in experiments. A flat surface is also set up to investigate exclusively the effect of van der Waals interaction between the CNT tip and the surface. The operating mode of a CNT-based probe is close to a tip-loaded cantilever. As illustrated in figure 1(a), the tip deflection Δx and load f is related by

$$f = k\Delta x \tag{1}$$

where k is the stiffness of the cantilever that is defined by the mechanical properties and geometrical parameters of a

cantilever

$$k \sim EIL^{-3} \sim d^4L^{-3}. \quad (2)$$

Here, d and L are respectively the diameter and length of the CNT probe. Inspired by this classical model, CNTs with various diameters and lengths are considered in the simulations to include the effects of bending stiffness, aspect ratio etc on imaging performance. CNTs simulated here include capped single-walled (6, 6), double-walled (6, 6)@(11, 11), and triple-walled (6, 6)@(11, 11)@(16, 16) nanotubes, which feature outermost diameters of 0.824 nm, 1.510 nm, and 2.196 nm respectively. The range of CNT lengths investigated here is from 4 to 12 nm.

Our molecular dynamics (MD) simulations are performed using the large-scale atomic/molecular massively parallel simulator (LAMMPS) code [15] and the DREIDING force field [16], where interactions between carbon atoms are described by Morse-type bond terms, harmonic cosine functions for bending angles, torsion terms, and a Lennard-Jones function for van der Waals interactions. The whole expression can be written as [17]

$$\begin{aligned} U(r_{ij}, \theta_{ijk}, \varphi_{ijkl}) = {} & K_{\mathrm{Cr}}\{\exp[-\gamma(r_{ij} - r_{\mathrm{C}})] - 1\}^2 \\ & + K_{\mathrm{C}\theta}(\cos\theta_{ijk} - \cos\theta_{\mathrm{C}})^2/2 \\ & + K_{\mathrm{C}\varphi}(1 - \cos 2\varphi_{ijkl})/2 + 4\varepsilon_{\mathrm{CC}} \\ & \times [(\sigma_{\mathrm{CC}}/r_{ij})^{12} - (\sigma_{\mathrm{CC}}/r_{ij})^6]. \end{aligned} \quad (3)$$

A cut-off $r_{\mathrm{cut}} = 1$ nm is used to truncate the van der Waals interactions. The potential functions and parameters used here are successfully applied to capture mechanical and vibrational properties of CNTs [17, 18]. The interactions between carbon atoms in the tip and copper atoms in the sample are calculated from the Lennard-Jones formula

$$U(r_{ij}) = 4\varepsilon_{\mathrm{C–Cu}}[(\sigma_{\mathrm{C–Cu}}/r_{ij})^{12} - (\sigma_{\mathrm{C–Cu}}/r_{ij})^6]. \quad (4)$$

The parameters here between the graphitic structure and copper surface are derived from density-functional theory (DFT) based calculations as reported before [19]. These parameters are verified by successfully predicting interface cohesive energies consistent with experimental data [20]. All parameters used in equations (3) and (4) are summarized in table 1. Since we focus on the behavior of CNT probes, the copper substrate is fixed during the scanning operation and surface vibrational effects that do not affect the assessment on the imaging quality of surface morphologies are neglected. The thickness of the substrate is larger than r_{cut}. Periodic boundary conditions are used in the lateral directions. To simulate the scanning process, the whole system is equilibrated in a Nosé–Hoover thermostat at 0.1 K in a vacuum. In experimental measurements there is continuous thermal fluctuation at finite temperature but it can be cancelled out by signal modulation [21]. Hence the use of these simulation conditions here is justified.

To simulate the scanning process of an AFM in CM, we utilize the steered molecular dynamics (SMD) technique, where a constant vertical load is applied on the top end of CNTs, i.e. a group of carbon atoms within 1 nm distance of the topmost atom (the fixed region shown in figure 1(a)). This group of atoms is integrated as a rigid body, and other atoms below represent the working part of the probe. Thus the torsional deformation of the cantilever is not considered here. The amplitude of the force is set to $P = 1$ nN that it is close to the one used in experiments. With a constant-force constraint, the constrained rigid end of a CNT is moved along in the ⟨100⟩ direction and starts to scan the surface. At the same time, the z-position (vertical) of the constrained group of atoms is written out as a measure for the height of the sample surface. In a minor digression, this causes the cantilever to deform and is typically detected optically afterwards. The ability to sense the deforming cantilever is recognized as the dynamic as opposed to the spatial resolution [22, 23]. Furthermore, since the practical working speed of an AFM is $l \sim 1\ \mu\mathrm{m\ s^{-1}}$, which is too low to be reached in atomistic simulations because of its high computation overhead, we utilize an alternative approach, where the CNT is moved by 0.1 nm with a speed of 1 m s^{-1} in each step, and then equilibrated for 200 ps before taking the next step to move. Dynamic effects of this method are excluded by comparing with slower scanning speeds.

Table 1. Force field parameters used in our MD simulations. (Note: K_{Cr}, $K_{\mathrm{C}\theta}$, $K_{\mathrm{C}\varphi}$, $\varepsilon_{\mathrm{CC}}$, r_{C}, γ, θ_{C}, σ_{CC} are taken from [17]. $\varepsilon_{\mathrm{CCu}}$ and σ_{CCu} are obtained through first-principles calculations [19].)

$K_{\mathrm{Cr}} = 478.9$ kJ mol^{-1}	$r_{\mathrm{C}} = 0.1418$ nm, $\gamma = 21.867$ nm^{-1}
$K_{\mathrm{C}\theta} = 562.2$ kJ mol^{-1}	$\theta_{\mathrm{C}} = 120°$
$K_{\mathrm{C}\varphi} = 25.12$ kJ mol^{-1}	
$\varepsilon_{\mathrm{CC}} = 0.4396$ kJ mol^{-1}	$\sigma_{\mathrm{CC}} = 0.3851$ nm
$\varepsilon_{\mathrm{CCu}} = 0.0447$ kJ mol^{-1}	$\sigma_{\mathrm{C–Cu}} = 0.22$ nm

3. Results and discussion

3.1. Instability during scanning by surface adhesion

To investigate the interaction between CNT tips and copper surfaces we first focus on a flat surface to exclude other complicated issues, as will be discussed later. As an AFM probe approaches the substrate at sub-nanometer distance, van der Waals interactions between the tip and the surface will generate forces on the probe during its scanning operation. As a result, the CNT will deform to reach an energetically favorable state under the load P, before starting to scan. The deformation caused by the load P and van der Waals interaction also affirms the premise of using the SFFM to depict a CNT acting as the probe [10]. Single-walled carbon nanotubes (SWNTs) with $L = 8$ and 10 nm are studied. Snapshots of the tip–surface configurations shown in figure 1(b) suggest remarkable deformation of the CNTs and significant dependence on the length of CNTs. It is obvious that both CNTs bend, but for $L = 10$ nm the CNT attaches to the surface after buckling. Although the bending deformation of the CNT with $L = 8$ nm is distinct, it still works in scanning by forming a tip–surface contact. However, for $L = 10$ nm, the friction force on the probe is enhanced and the relationship between CNT deformation and the surface morphology can hardly be mapped.

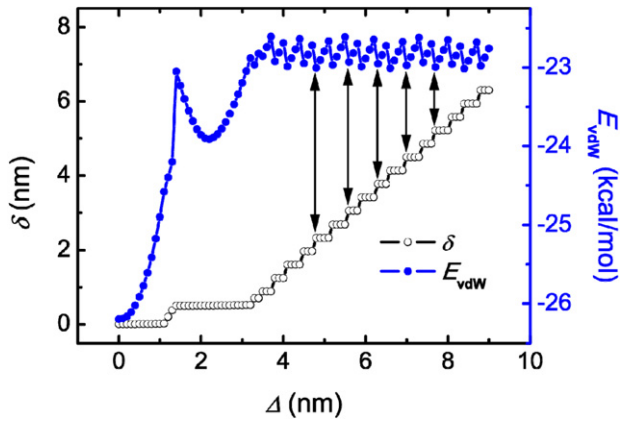

Figure 2. Dependence of the probe tip displacement δ along the scanning direction and van der Waals interaction energy E_{vdW} on probe root displacement Δ. Here, the probe is a SWNT 8 nm in length and the surface is flat. Both δ and E_{vdW} curves reach relatively stable profiles after Δ exceeds ~3.5 nm. The probe tip displacement δ shows a step-like pattern and each jump corresponds to a period in the changes of the van der Waals interaction energy profile as guided by the double-headed arrows.

3.2. Surface effects with atomistic discreteness

We thus focus on the CNT with $L = 8$ nm here for deeper insights into the tip–surface interaction. The rigid part of the CNT is moved by a displacement Δ in our simulations and the displacement δ of the CNT tip in the scanning direction δ is tracked, as shown in figure 2 together with van der Waals interaction energy E_{vdW} between the CNT and surface. The results show that δ reaches a relatively stable state with a step jump after Δ approaches approximately 3.5 nm. We define the lag in displacement $d_{phase} = \delta - \Delta$ as the phase shift here. In figure 2 we also notice that E_{vdW} experiences similar variation pattern as δ, i.e. any step jump in the displacement of the CNT tip corresponds to a step change in its interaction energy with the surface, as indicated by double-headed arrows. We calculate the period x_p of their variation by averaging over the last 17 scanning cycles in figure 2. We find that $x_p = 0.36$ nm, which is consistent with the lattice constant $a_{Cu} = 0.361$ nm of a copper (001) surface. This suggests that the variation pattern originates from the discrete nature at the atomic scale, which creates energy barriers between adjacent lattice points in copper. This behavior constitutes an example indicating the breakdown of continuum models for mechanical contacts that have been found to be affected by surface roughness [24]. As a result, before moving to the next lattice point, a CNT probe needs to deform, e.g. bend, to accumulate enough energy in elastic deformation in order to overcome the barrier. This eventually leads to the phase shift d_{phase} and the tip's step jump movement pattern. The results shown here reveal that the load P, adhesive interaction between the CNT tip and the surface, is responsible for deformation of the probe as observed in the simulations (figure 1(b)) and becomes a vital first step in practical applications of probes that are stiff enough to resist surface adhesion.

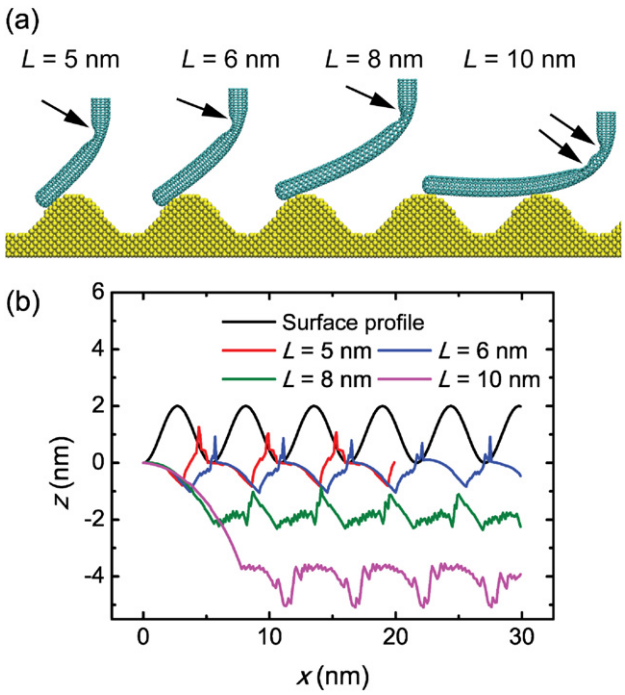

Figure 3. (a) Deformation of SWNTs with $d = 0.824$ nm and $L = 5$, 6, 8, and 10 nm during scanning a sinusoidal surface, where $2A = 2$ nm and $\Lambda = 5.415$ nm. Buckling behaviors (indicated by black arrows) are observed for all probes, and for $L = 10$ nm the SWNT stretches over two ridges with a twin-buckling behavior. (b) Comparison between surface profile and scanning outputs using SWNTs ($d = 0.824$ nm) with different lengths, which shows that shorter probes perform better in reproducing the surface topology.

3.3. Nonlinear buckling and sensitivity to surface fluctuation

As the effect of surface adhesion on the deformation of CNT tips is identified, its impact on the imaging quality is now addressed. Here, we introduce a sinusoidal profile $H = A\sin(2\pi x/\Lambda)$ to represent the general surface morphology, while also being simple enough for quantitative analysis. The sample surface has height H varying with maximum amplitude $2A = 1$ nm and a wavelength $\Lambda = 5.415$ nm that is 15 times a_{Cu}, the lattice constant of copper. To identify the performance of CNT probes, SWNTs with lengths $L =$ 5, 6, 8, and 10 nm and double-walled CNTs (DWNTs) with lengths $L = 6$, 8, and 10 nm are considered in our simulations. Snapshots of the SWNTs as they cross the ridge of the surface are plotted in figure 3(a). It is noticed that all SWNTs bend to the extent of buckling. When $L =$ 10 nm, rippling or buckling with two local instabilities is observed, which can be attributed to its slightly lowered stiffness k [25, 26]. Along with the rippling, the 10 nm long SWNT also lies over two adjacent ridges. This phenomenon is reminiscent of our previous observation on the flat surface for SWNTs with $L = 10$. Correspondingly, figure 3(b) plots the topology (height) profiles as measured by lateral scanning using SWNTs of different lengths. Clearly, the shorter tubes perform better, although not likely to be satisfied in a practical scenario. The trend can be conclusively attributed to the enhancement of stiffness in shorter CNTs as in a cantilever

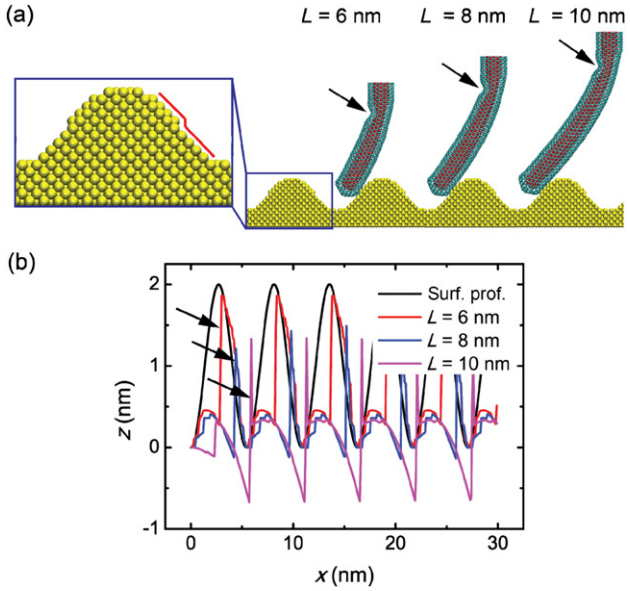

Figure 4. (a) Deformation of DWNTs ($d = 1.510$ nm) with $L = 6$, 8, and 10 nm during scanning a sinusoidal surface, where $2A = 2$ nm and $\Lambda = 5.415$ nm. Buckling behaviors are observed for all nanotubes. As the length scale reaches sub-nanometer the atomic discreteness yields step changes on the surface (outlined by the red line in the inset). (b) Comparison between surface profile and scanning outputs using DWNTs ($d = 1.510$ nm) with different lengths, which shows step responses (see arrows in the figure) originating from atomic surface roughness (see the inset in panel (a)).

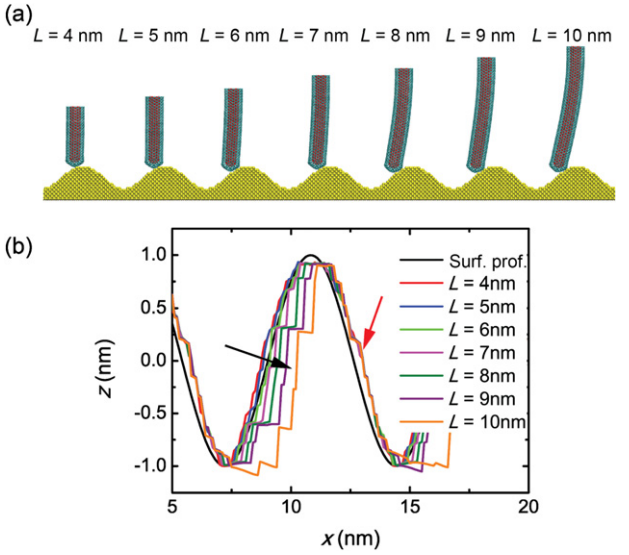

Figure 5. (a) Deformation of DWNT probes ($d = 1.510$ nm) with different lengths from 4 to 10 nm during scanning of a sinusoidal surface, where $2A = 2$ nm and $\Lambda = 7.22$ nm. The smaller amplitude–wavelength ratio $2A/\Lambda$ here excludes perturbation from sharp edges (see the inset in figure 4(a)). None of the probes here experience buckling any more. (b) Comparison between surface profile and scanning outputs using DWNTs of different lengths. It is shown that longer probes have deeper indentation at the windward sections (indicated by the black arrow), while all the curves overlap each other at the leeward sections (indicated by the red arrow). The black arrow also indicates the trend of data as the length of carbon nanotubes L increases from 4 to 10 nm.

model. Figure 4(a) shows the deformation of DWNTs as they cross the surface's ridge. Similar to SWNTs, buckling occurs in all DWNTs, but with reduced radial deformations in comparison with SWNTs as shown before in figure 3(a). Also, the DWNT with $L = 10$ nm does not show a rippling feature, as attributed to the much enhanced stiffness k with a larger diameter and double-walled nature, where the outer wall is constrained by the inner one [26]. Figure 4(b) plots the surface profiles measured by these DWNTs. Similarly to SWNTs, longer DWNTs always gives worse mapping of the surface morphology, as compared with the original profile. Moreover, the measured curves exhibit step responses as denoted by arrows in figure 4(b). A closer examination of the atomic structure of the copper surface uncovers the origin of this phenomenon. As evidenced in the inset, the step change in the profile output comes from the discreteness of surface atoms. One can also see in our MD simulations that the DWNTs bend severely due to restriction from sharp edges, and a sudden release phenomenon will occur when the nanotube deforms significantly to overcome this restriction. This phenomenon of sudden release, similar to the step jump movement pattern as discussed above, leads to the step-like response. This behavior indicates that the performance of CNT tips is sensitive to the atomic-scale corrugation of the surface. Any step change in the surface topography could result in step-like response in the signal output from measurements that distort the whole curve and prevent sub-atomic-scale imaging of surfaces using AFMs. Moreover, the structure of the substrate surface is important for establishing the validity of the breakdown of the contact laws with the nanotube. Detailed structural information such as surface reconstruction that changes the surface–probe interaction, defects and adsorption of guest molecules could also modify the measured data for surface topology in a similar manner to that discussed above.

3.4. The critical role of stiffness

In order to validate the performances of CNT probes by considering the effect of their diameters and lengths, a smoother surface was introduced that ameliorates the influence of the atomic-scale corrugation as discussed above. The amplitude $2A$ and wavelength Λ of the sinusoidal surface profile are 1 nm and 7.22 nm or $20a_{\mathrm{Cu}}$, respectively. DWNTs with $L = 4, 5, 6, 7, 8, 9$, and 10 nm are used in our simulations. Figure 5(a) shows the deformation of these DWNTs while they cross the ridges on the surface. Compared to former snapshots in figure 4(a), none of the DWNTs here show buckling behaviors because of the relatively smoother profile. This result also accounts for the sensitivity of CNT probes to surface fluctuation as discussed in the previous section. Figure 5(b) plots the profiles as traced out by these DWNTs in comparison with the original one. As shown here, these curves reproduce well the original surface topography, and could be analyzed in a quantitative way to map back from measured data in experiments. Here we fit the measured profiles using a sinusoidal function

$$z = A\sin[2\pi(x - d_{\mathrm{phase}})/\lambda - \pi/2] + B \qquad (5)$$

through a nonlinear least squares fitting technique, where λ is the wavelength of the original curve, d_{phase} is the phase shift between the measured and original profile, A is the fitted height of the surface and B is a constant shift of the measured data. From the fitted results we also define a root-mean-square error (RMSE), which is associated with the best-fit curve and the original profile, as an indicator showing the capability of CNT tips to reproduce the sinusoidal surface topography. These parameters provide indicative benchmarks for the scanning integrity. The phase shift and RMSE are plotted as a function of length of several DWNTs in figure 6(a). It is clearly shown that d_{phase} increases with L monotonically, while RMSE varies with a non-monotonic trend. The variation of d_{phase} could be simply explained by the fact that longer CNTs experience larger deformation prior to scanning, while the variation of RMSE can be explained by data shown in figure 5(b). For convenience, we annotate the sections in the scanned profile that faces and leaves the probe in the direction of scanning as windward and leeward sections following conventions in sailing. As highlighted by black arrows in figure 5(b), deviations from fitted curves appear more frequently at the windward sections of the ridges in the surface—when they are almost overlapping each other—than at the leeward sections. Also since windward sections lie in the direction of scanning, the deformation of the CNT tip results more from the probe encountering ridges as an obstacle than from the adhesion between the tube's tip and the surface. This effect was previously discussed by Carpick *et al* [4], where a calibration technique is also presented. At the leeward sections, all measured profiles show almost the same deviations from the original one. This is a consequence of the convolution effect that has been demonstrated previously in conventional silicon and silicon nitride AFM probes [3, 27]. When L is reduced to a value at which the CNT tip is stiff enough and experiences very small deformations, the convolution effect starts to present in windward sections. As an example, the measured curve for the DWNT with $L = 4$ nm displays a convolution effect at windward sections.

Besides the length L of the CNT that defines stiffness k, its diameter d also plays a critical role through the second moment of the area I for any specific length L. Guided by equation (2), more MD simulations using CNTs of different diameters and lengths are carried out to investigate the role of k more generally, including SWNTs with $L = 6$ and 8 nm and triple-walled carbon nanotubes (TWNTs) with $L = 8$, 10, and 12 nm. The best-fit procedure is applied, and the phase shift d_{phase} and RMSE as calculated are shown in figure 6(b) with the effective stiffness d^4L^{-3} as an independent variable. Similar variation is observed here as in figure 6(a), but this result validates the tip-loaded cantilever model as shown in figure 1(a), and the effective stiffness defined in equation (2) can be used to design CNT tips for AFM probes in practice. By comparing these simulation results and those with different A/Λ values (figures 3 and 4), we find that buckling of CNT probes becomes less favorable for smoother surfaces, and its dependence on these geometrical parameters remains the same. As demonstrated by figure 6(b), both the phase shift and RMSE fall dramatically with increasing

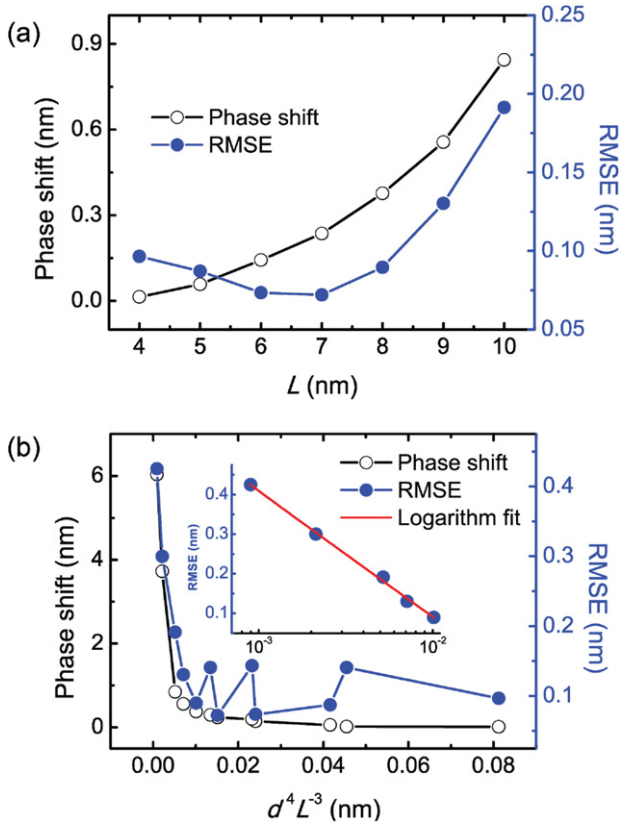

Figure 6. The phase shift and RMSE during surface scanning using CNT-based probes, where $2A = 2$ nm and $\Lambda = 7.22$ nm. (a) The phase shift and RMSE based on the outputs of DWNTs vary with tube length. (b) The dependence of phase shift and RMSE on the effective stiffness d^4L^{-3}. Besides the DWNTs in panel (a), the CNT probes used here include SWNTs with $L = 6$ and 8 nm and triple-walled carbon nanotubes (TWNTs) with $L = 8$, 10, and 12 nm. Both these variables reach a plateau rapidly after a dramatic drop. The inset replots the first five records of RMSE on a logarithmic scale, which shows that the reduction of RMSE as a function of the effective stiffness follows a logarithmic law.

effective stiffness d^4L^{-3} and reach a plateau rapidly. Also, the RMSE fluctuates after the dramatic drop. It is a result of the presence of the convolution effect as the stiffness reaches a relatively larger value, which is consistent with the previous discussion on tube length. Getting closer to the results, the first five records are plotted in the inset of figure 6(b) with a logarithmic abscissa. It shows that the RMSE decrease as functions of the effective stiffness in a logarithmic law $\mathrm{RMSE} = -0.138\ln(d^4L^{-3}) - 0.5456$, which suggests that one does not need to increase the stiffness of tips excessively to minimize errors in AFM imaging.

4. Conclusion

By performing MD simulations, we revealed the correlation between the mechanical behavior of CNTs used as AFM probes operating in contact mode and its impact on imaging performance. Since the CNT tip contacts the sample surface directly, van der Waals interaction between them dominates and accounts for the lateral load on the tip. For relatively

flexible CNT-based probes, strong adhesion is observed that results in instability through elastic buckling, resulting in severe errors in the images of the surface topography. Atomic-scale surface corrugation effects, which result from a breakdown of the continuum models for mechanical contacts, were also found to play a deleterious role. In the presence of these effects it will not be possible to derive reliable surface information from the scanned data. Consequently, the design of CNT-based probes in AFMs requires considerable stiffness of the tip in order to avoid instabilities and errors from lattice discreteness. When this is done, we verified that the developed tip-loaded cantilever model is suitable for accurate prediction and showed that both the error metrics of phase shift and the RMSE decrease with probe stiffness according to a logarithmic law. This logarithmic law importantly infers an ability to minimize the imaging error without the need to increase the stiffness excessively. The results here also shed some light on the design of CNT-based nanomanipulators that operate through van der Waals interactions between CNTs and target objects in which large deformation and instability of the CNTs are expected [28].

Acknowledgments

We thank Professor Qunyang Li for critical reading and discussion. This work was supported by Tsinghua University Initiative Scientific Research Program 2011Z02174, the National Natural Science Foundation of China (grant nos 11002079 and 10972121), and the Tsinghua National Laboratory for Information Science and Technology, China. TW expresses gratitude for funding support from the Australian Research Council's DP120100583 grant.

References

[1] Binnig G, Quate C F and Gerber C 1986 *Phys. Rev. Lett.* **56** 930–3
[2] Chen Y, Wilson I H, Lee C, Xu J and Yu M 1997 *J. Appl. Phys.* **82** 5859–61
[3] Bukharaev A A, Berdunov N V, Ovchinnikov D V and Salikhov K M 1998 *Scanning Microsc.* **12** 225–34
[4] Ogletree D F, Carpick R W and Salmeron M 1996 *Rev. Sci. Instrum.* **67** 3298–306
[5] Poncharal P, Wang Z, Ugarte D and de Heer W A 1999 *Science* **283** 1513–6
[6] Nishio M, Akita S and Nakayama Y 2005 *Japan. J. Appl. Phys.* **44** 1097–9
[7] Dai H, Hafner J H, Rinzler A G, Colbert D T and Smalley R E 1996 *Nature* **384** 147–50
[8] Wilson N R and Macpherson J V 2009 *Nature Nanotechnol.* **4** 483–91
[9] Cheung C L, Hafner J H and Lieber C M 2000 *Proc. Natl Acad. Sci. USA* **97** 3809–13
[10] Ishikawa M, Yoshimura M and Ueda K 2002 *Physica* B: *Condens. Matter* **323** 184–6
[11] Chen L, Cheung C L, Ashby P D and Lieber C M 2004 *Nano Lett.* **4** 1725–31
[12] Nguyen C V, Ye Q and Meyyappan M 2005 *Meas. Sci. Technol.* **16** 2138–46
[13] Ishikawa K and Cho Y 2006 *Rev. Sci. Instrum.* **77** 103708
[14] Kutana A, Giapis K P, Chen J Y and Collier C P 2006 *Nano Lett.* **6** 1669–73
[15] Plimpton S 1995 *J. Comput. Phys.* **117** 1–19
[16] Guo Y J, Karasawa N and Goddard W A 1991 *Nature* **351** 464–7
[17] Walther J H, Jaffe R, Halicioglu T and Koumoutsakos P 2001 *J. Phys. Chem.* B **105** 9980–7
[18] Chen C, Ma M, Jin K, Liu J Z, Shen L, Zheng Q and Xu Z 2011 *Phy. Rev.* E **84** 046314
[19] Xu Z and Buehler M J 2010 *J. Phys.: Condens. Matter* **22** 485301
[20] Yoon T, Shin W C, Kim T Y, Mun J H, Kim T S and Cho B J 2012 *Nano Lett.* **12** 1448–52
[21] Kobayashi K, Yamada H and Matsushige K 2009 *Rev. Sci. Instrum.* **80** 043708
[22] Ng T W, Sasaki O and Chua H 2004 *Opt. Eng.* **43** 75–8
[23] Ng T W and Panduputra Y 2012 *Langmuir* **28** 453–8
[24] Luan B and Robbins M O 2005 *Nature* **435** 929–32
[25] Liu J Z, Zheng Q and Jiang Q 2001 *Phys. Rev. Lett.* **86** 4843–6
[26] Nikiforov I, Zhang D-B, James R D and Dumitrica T 2010 *Appl. Phys. Lett.* **96** 123107
[27] Grow R J, Minne S C, Manalis S R and Quate C F 2002 *J. Microelectromech. Syst.* **11** 317–21
[28] Suga H, Naitoh Y, Tanaka M, Horikawa M, Kobori H and Shimizu T 2009 *Appl. Phys. Exp.* **2** 5004-3